

Silver Flakes and Silver Dendrites for Hybrid Electrically Conductive Adhesives with Enhanced Conductivity

HONGRU MA,^{1,2,3} ZHUO LI,⁴ XUN TIAN,^{2,3} SHAO CUN YAN,^{2,3} ZHE LI,^{2,3}
XUHONG GUO,^{3,5} YANQING MA,^{1,6} and LEI MA^{2,7}

1.—School of Precision Instrument and Opto-Electronics Engineering, Tianjin University, Tianjin 300072, People's Republic of China. 2.—Tianjin International Center for Nanoparticles and Nanosystems, Tianjin University, Tianjin 300072, People's Republic of China. 3.—School of Chemistry and Chemical Engineering, Shihezi University, Shihezi 832003, People's Republic of China. 4.—Department of Materials Science, Fudan University, 220 Handan Road, Shanghai 200433, People's Republic of China. 5.—State Key Laboratory of Chemical Engineering, East China University of Science and Technology, Shanghai 200237, People's Republic of China. 6.—e-mail: mayanqing@tju.edu.cn. 7.—e-mail: lei.ma@tju.edu.cn

Silver dendrites were prepared by a facile replacement reaction between silver nitrate and zinc microparticles of 20 μm in size. The influence of reactant molar ratio, reaction solution volume, silver nitrate concentration, and reaction time on the morphology of dendrites was investigated systematically. It was found that uniform tree-like silver structures are synthesized under the optimal conditions. Their structure can be described as a trunk, symmetrical branches, and leaves, which length scales of 5–10, 1–2 μm , and 100–300 nm, respectively. All features were systematically characterized by scanning electron microscopy, transmission electron microscopy (TEM), high-resolution TEM, and x-ray powder diffraction. A hybrid fillers system using silver flakes and dendrites as electrically conductive adhesives (ECAs) exhibited excellent overall performance. This good conductivity can be attributed mainly to the synergy between the silver microflakes (5–20 μm sized irregular sheet structures) and dendrites, allowing more conductive pathways to be formed between the fillers. In order to further optimize the overall electrical conductivity, various mixtures of silver microflakes and silver dendrites were tested in ECAs, with results indicating that the highest conductivity was shown when the amounts of silver microflakes, silver dendrites and the polymer matrix were 69.4 wt.% (20.82 vol.%), 0.6 wt.% (0.18 vol.%), and 30.0 wt.% (79.00 vol.%), respectively. The corresponding mass ratio of silver flakes to silver dendrites was 347:3. The resistivity of ECAs reached as low as $1.7 \times 10^{-4} \Omega \text{ cm}$.

Key words: Silver flake, silver dendrites, hybrid fillers system, replacement reaction, electrically conductive adhesives

INTRODUCTION

Electronic packaging, the technology of mechanically and electrically interconnecting a multiplicity of components into an integrated system, has been dominated by tin/lead based solders for a long time.¹

However, due to the toxicity of lead and its effect on human health, many countries, such as Japan and the European Union, have either completely banned or minimized its usage. In past decades, extensive efforts have been paid to developing environmentally friendly alternatives for lead-containing solders.²

In the field of electrically conductive adhesives (ECAs), the most promising lead-free candidate

(Received December 31, 2016; accepted February 14, 2018; published online March 2, 2018)

materials for soldering in modern electronics³ are generally composed of two main components: a polymer matrix and conductive fillers. The polymer matrix provides mechanical interconnection and the conductive fillers provide the required electrical conductivity. Different types of materials such as gold, silver, nickel, copper, graphite and carbon nanotubes have been used as conductive fillers of ECAs.^{4–8} Among the various conductive fillers, silver is the most commonly used, due to its excellent conductivity, as well as its thermal and chemical durability.⁹ Conventional ECAs (epoxy and silver flakes) offer several advantages over the traditional lead-based solders, such as environmental friendliness, milder operating conditions, fewer process steps etc.¹⁰ However, the complete replacement of traditional solders with conventional ECAs has not yet been achieved because of their relatively low electrical conductivity. Usually, the conventional ECAs possess rather high bulk resistivity compared to the metal, which limits their application in many fields, especially in precision manufacturing and microelectronic packaging.^{3,11} It would seem that more silver flakes in epoxy would lead to higher electrical conductivity of the conventional ECAs, but this is not always true. Specifically, after the electric network percolation threshold of the filler has been reached, the network becomes stable, and more silver flakes have only negligible effects on electric conductivity, while severely deteriorating the mechanical properties of the ECAs and dramatically increasing the material cost.¹²

Therefore, it is essential to seek better filler systems that not only can effectively improve the electrical properties of the ECAs but also have no need to increase the amount of conductive fillers. This requires maximizing the conductive pathways while minimizing the quantity of conductive fillers.

Recent reports show rapidly growing interest in the use of hybrid fillers for ECAs.¹³ Silver nanostructures of varying sizes and shapes have been widely introduced into conventional ECAs to improve their electrical conductivity. Normally, the utilization of these nanomaterials as auxiliary fillers in the conventional ECAs yields a synergetic effect between silver nanomaterials and silver flakes, effectively improving electrical conductivity.¹⁰ The incorporation of silver nanoparticles into systems of epoxy and silver flakes to develop new hybrid filler systems has been studied by several groups. Qiao et al.¹⁴ incorporated silver nanoparticles into ECAs, finding that silver nanoparticles can effectively fill the gaps between the silver flakes and form a conductive network, enhancing the conductivity of the ECAs. However, some subsequent research results are still controversial. Fan et al.¹⁵ and Mach et al.¹⁶ reported that silver nanoparticles have negative effects on electrical conductivity. On the other hand, Zhang et al.¹⁷ reported on hybrid filler systems of high aspect-ratio silver nanowires

as auxiliary fillers in the conventional ECAs, resulting in significant improvement in electrical conductivity. Chen et al.¹⁸ incorporated silver nanowires into ECAs in which silver microparticles were used as a conductive fillers, which also showed that a doped system had much better electrical conductance compared to an un-doped one with the same amount of silver fillers.

In this paper, we report the incorporation of silver dendrites, a new class of high aspect-ratio silver fillers, into a conventional ECA to develop a hybrid ECAs composite. The structure of silver dendrites has received extensive attention in the last few years. They are widely used in such diverse applications as sensors,¹⁹ catalysis,²⁰ surface enhanced Raman scattering,²¹ and have gradually been applied to the electronics industry.²² Many approaches have been reported for yielding silver dendrites, such as electrochemical deposition,^{23–25} wet-chemical route,^{26,27} solvothermal method,²⁸ ultrasonic-assisted reduction,²⁹ template assistant method,^{30,31} and oxidation reduction reaction.²² However, most reported synthetic methods involve many steps and rather complicated procedures, including employment of reductants, with the requirements of high temperatures and template/substrate removal in the last step in order to purify the final products. Some of those reductants are toxic, such as sodium borohydride, which is not only dangerous but also environmentally unfriendly. Here, we synthesized silver dendrites by a simple replacement reaction,^{32,33} a method that is relatively simple and very environmentally friendly. The simplicity of this method means that no complicated equipment or special reagents are needed. Compared to the conditions for synthesizing high aspect-ratio silver nanowires, the conditions for fabricating silver dendrites are simple, fast and very mild.

In the present study, ECAs are filled with silver flakes and silver dendrites in order to develop binary Ag/epoxy adhesives. The silver dendrites possess the key features of an ideal conductive filler for ECAs. The high aspect-ratio of silver dendrites can very efficiently establish many stable and effective conductive networks at very low filler content.^{34,35} The electrical properties of the ECAs filled with hybrid fillers are discussed in terms of the mass fraction of conductive fillers. The ECAs filled with silver flakes and dendrites demonstrate excellent conductivities in comparison with the rest of the ECA family.

EXPERIMENTAL SECTION

Chemicals and Reagents

Zinc powder with particle size of $\sim 20 \mu\text{m}$ was purchased from Tianjin Fuchen Chemical reagents factory. Silver nitrate was obtained from Xi'An Chemical Corporation. The silver microflakes (irregular sheet structure with size about $5\text{--}20 \mu\text{m}$)

were acquired from Strem Chemicals, Inc. 1-(2-Cyanoethyl)-2-ethyl-4-methylimidazole (2E4MZ-CN) and 4-Methylcyclohexane-1, 2-dicarboxylic Anhydride (MHHPA) were supplied by TCI (Shanghai) Development Co. Ltd. Hydrochloric acid (HCl, 38%) and ethanol were supplied by Tianjin Fuyu Fine Chemical Co. Ltd. Nitric acid (HNO₃, 65–68%) was ordered from Chengdu Kelong Chemical Reagent Factory. All chemicals and reagents were

analytical grade or above without further purification for use.

Synthesis of Silver Dendrites

The silver dendrites were prepared by a conventional replacement reaction. The zinc powder was first treated with hydrochloric acid and later washed with distilled water to remove surface contamination. The treated zinc powder was dis-

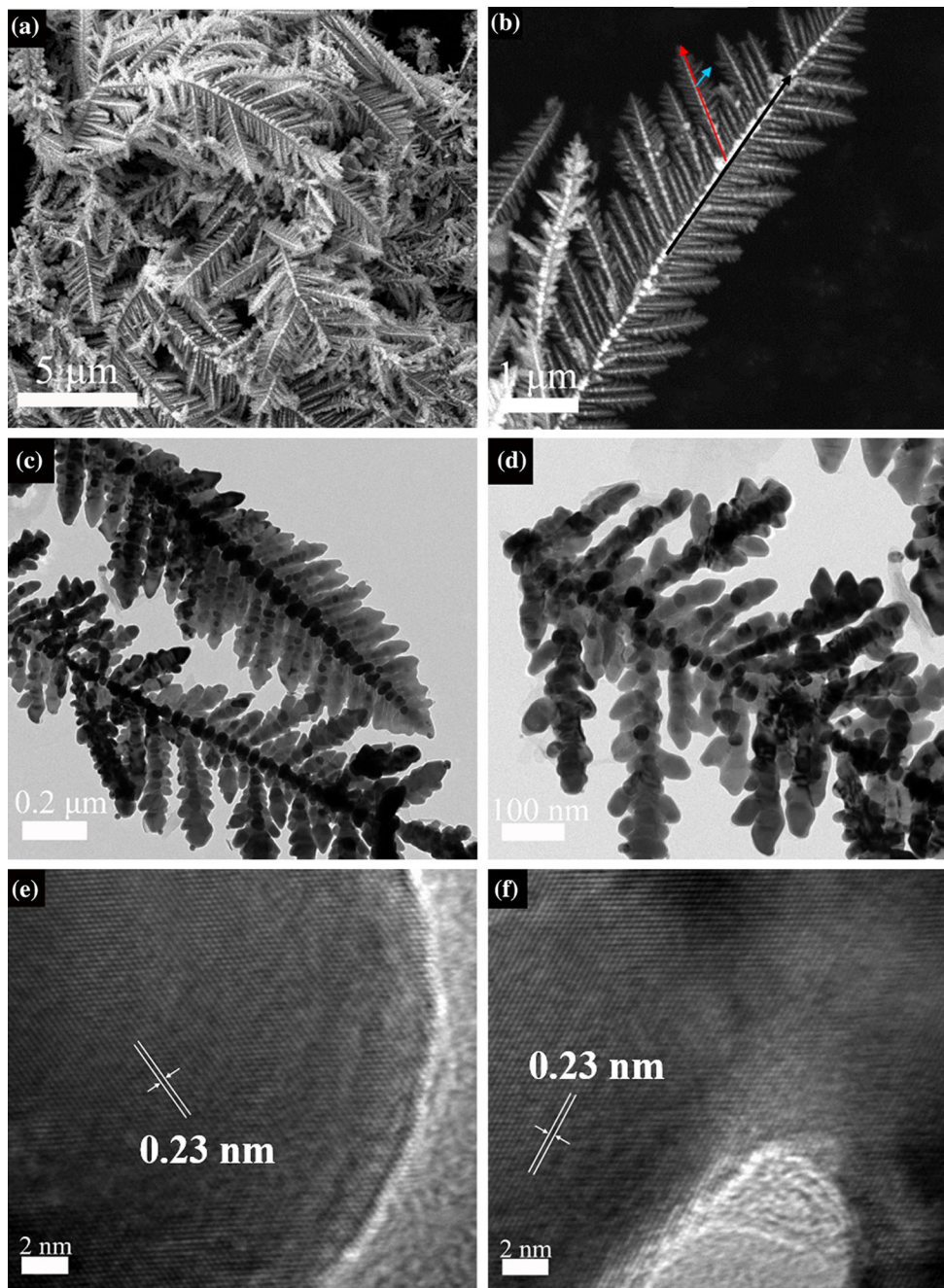


Fig. 1. (a, b) SEM images of the silver dendrites at different magnifications. (c, d) TEM images of the silver dendrites at different magnifications. (e) HRTEM image of the Ag trunk. (f) HRTEM image of the silver dendrites at a connection site between the trunk and one of its branches.

persed into ethanol and then ultrasonicated for 30 min. The zinc powder suspension was dropped into the AgNO_3 solution with gentle stirring and the whole reaction was performed under ambient conditions. The resulting silver dendrites were washed with 0.5 M dilute nitric acid to take off the residual zinc powder and then further washed with distilled water and ethanol, successively. Finally, the product was collected for characterization. In order to obtain a complete, symmetrical and uniform tree-like silver structure, we varied several reaction conditions for investigation of the influence of the

experimental parameters on the morphology of the silver dendrites.

Preparation of ECAs

The polymer matrix consisted of an epoxy resin (density 1.2 g/cm^3), a curing agent (MHHPA) and a catalyst (2E4MZ-CN). Their weight ratios were 1:0.85:0.0185. When the silver flakes and purified silver dendrites were added into the polymer matrix, the total amount of conductive fillers was 70.0 wt.% (21.00 vol.%) (see Supplementary Tables S1 and S2). The composite was stirred for 2 h and then ultrasonicated for 0.5 h in order to disperse the conductive fillers evenly through the epoxy resin. Two strips of polyimide tape were applied onto a pre-cleaned glass slide with a gap of 3 mm. The mixed composite was pasted uniformly into the gap between the two strips. Later, the polyimide tape was removed from the glass slide and the ECA was then cured at 150°C for 2 h.

Characterization

The morphology of silver dendrites was characterized with a scanning electron microscope (SEM) (JSM-6490LV) from JEOL, and transmission electron microscopy (TEM) images were obtained from an FEI Tecnai G20 transmission electron microscope. X-ray diffraction (XRD) (Bruker D8 advanced x-ray diffractometer) was used for determination of

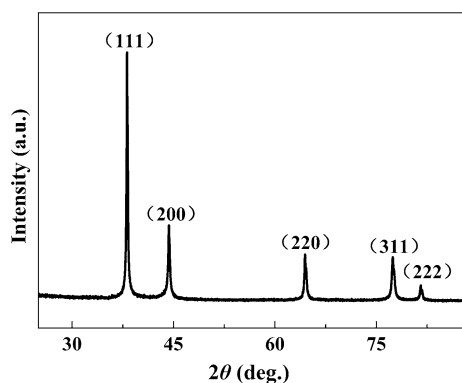


Fig. 2. XRD pattern of as-synthesized silver dendrites.

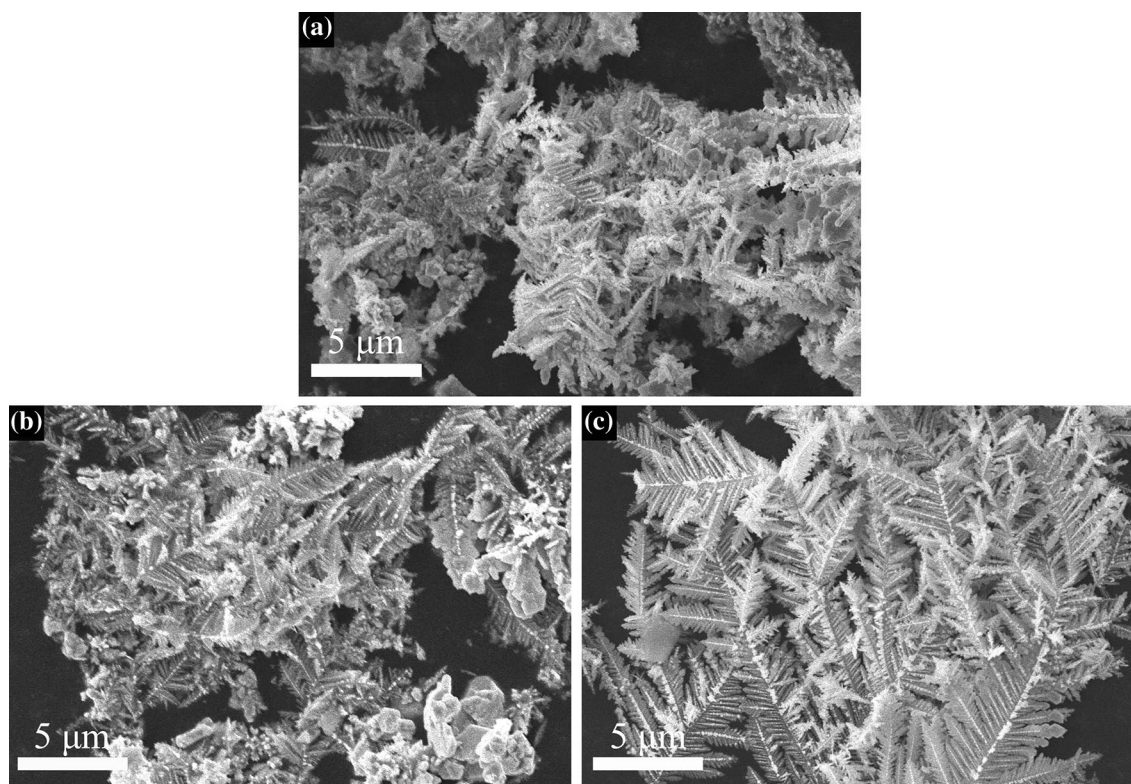


Fig. 3. SEM images of silver dendrites grown at the following molar ratios of silver nitrate and zinc powder: (a) 1:1, (b) 2:1, and (c) 4:1. Other experimental parameters are the same, reaction solution volume is 40 mL, silver nitrate concentration is 30 mM, and reaction time is 6 h.

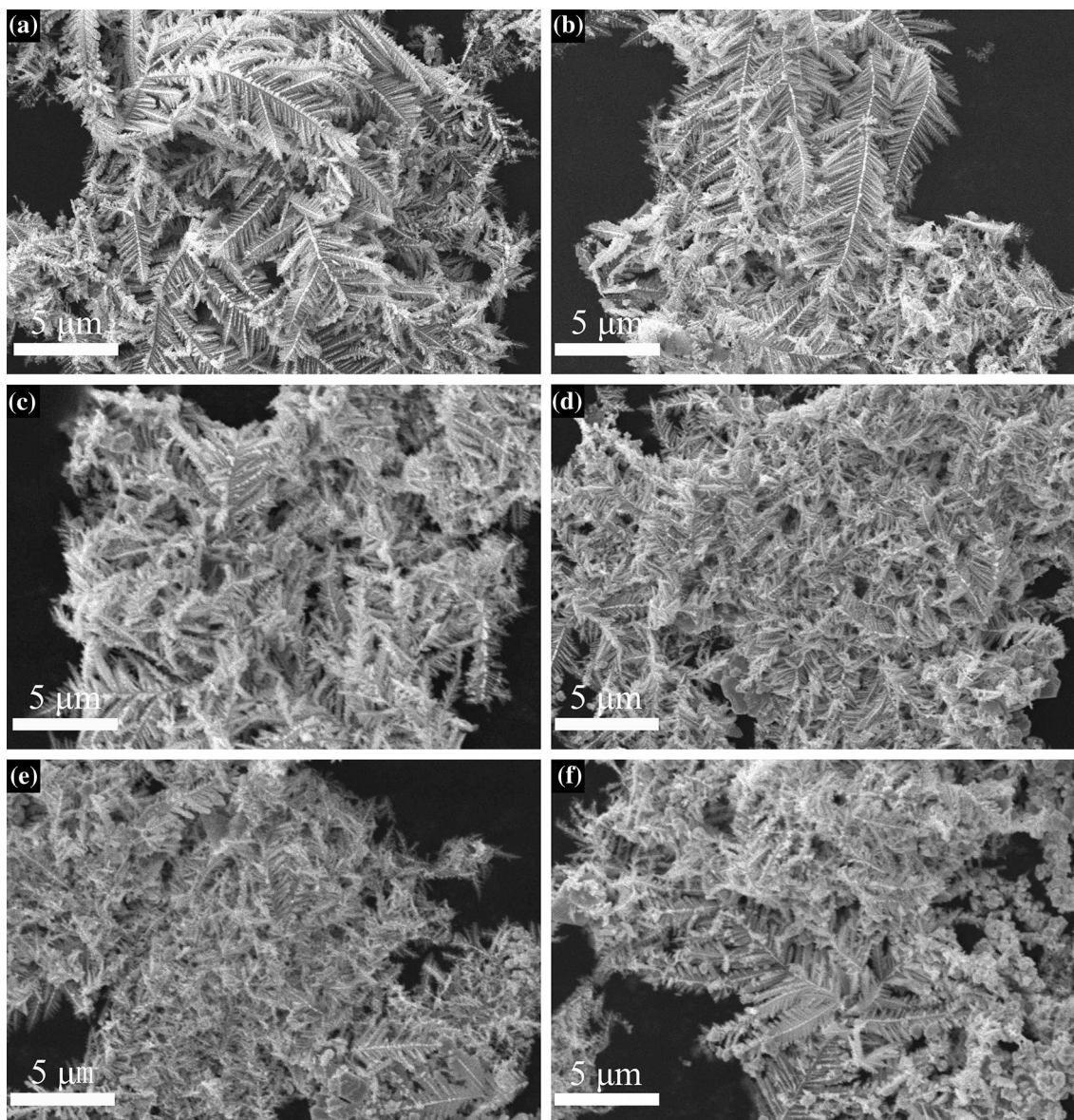


Fig. 4. SEM images of Ag dendrites grown at the following volumes of reaction solution: (a) 40 mL, (b) 60 mL, (c) 100 mL, (d) 120 mL, (e) 140 mL, and (f) 160 mL. Other experimental parameters are the same, reactant molar ratio is 4:1, silver nitrate concentration is 30 mM, and reaction time is 6 h.

the crystalline structure of silver dendrites. The sheet resistance of the ECAs was measured using a RTS-8 four-point probe meter (Guangzhou Electronic Technology Ltd.). The probe material was high-speed steel. The four electrical contacts were in a straight line and the distance between electrical contacts was 1 mm. The thickness of samples was measured by a thickness gauge (Shanghai Chuanlu Measuring Tools Co. Ltd.). The resistivity ρ was calculated using Eq. 1:

$$\rho = R_L \times T, \quad (1)$$

where R_L and T are sheet resistance and thickness of the sample, respectively. In order to minimize random errors in the measurements of sample resistivity, the average of five measured values

was considered as the closest one to the real resistivity.

RESULTS AND DISCUSSION

As described above, the morphology of the obtained silver dendrites was characterized by an SEM (Fig. 1a and b). The SEM image shows that silver dendrites structures are mainly composed of three parts: the black arrow represents the trunk (first branch), the red dashed arrow indicates the branch (secondary branch), and the blue arrow is the leaf (tertiary branch). The trunk is about 5–10 μm in length, the branch is around 1–2 μm long, and the leaf with the size scale of 100–300 nm. Additionally, each dendrite is symmetrical, and the trunk and branch have the angles between 50°–60°.

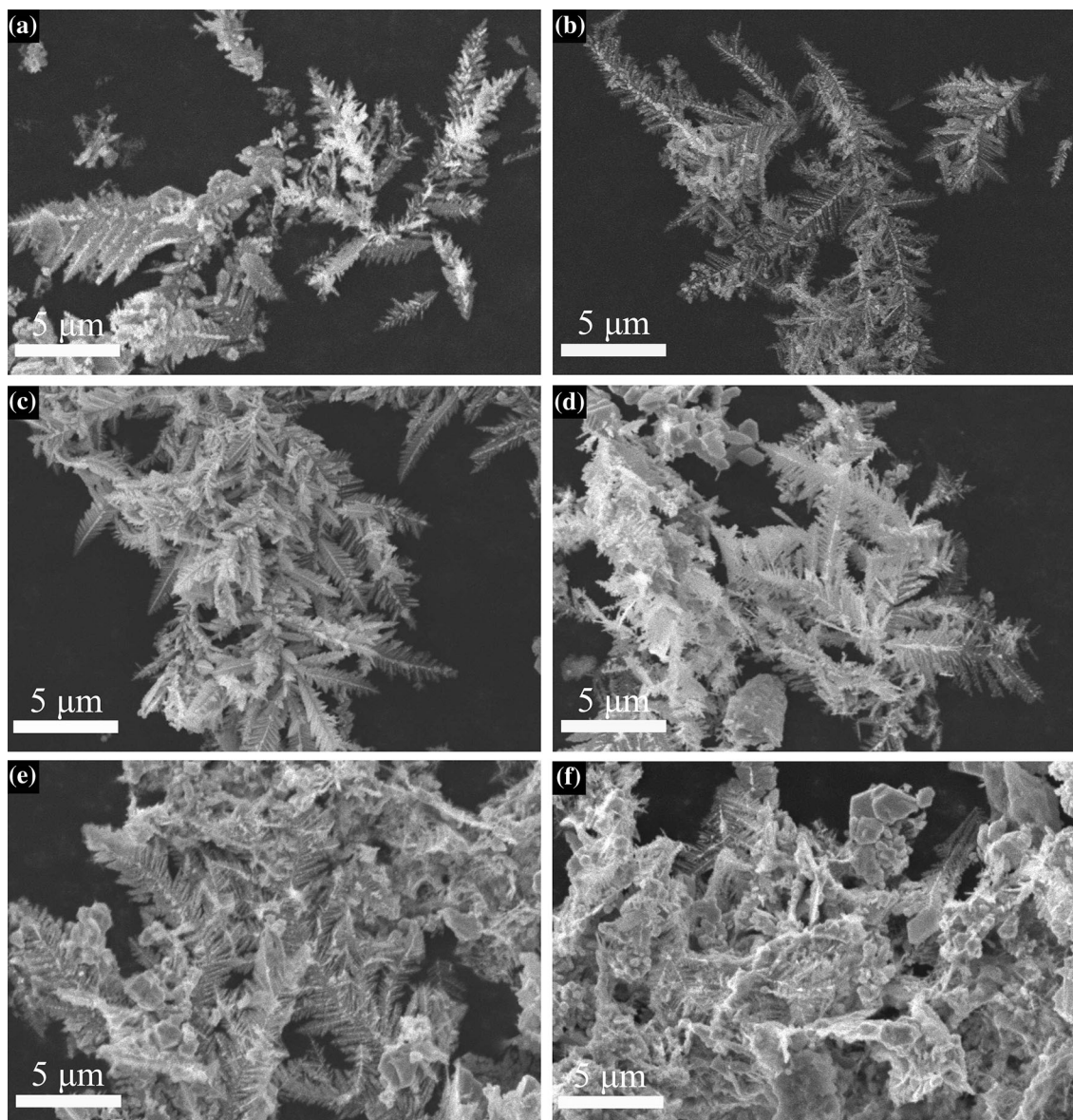


Fig. 5. SEM images of the silver dendrites grown at the following AgNO_3 concentrations: (a) 5 mM, (b) 15 mM, (c) 30 mM, (d) 50 mM, (e) 100 mM, and (f) 200 mM. Other experimental parameters are the same, reactant molar ratio is 4:1, reaction solution volume is 40 mL, and reaction time is 6 h.

TEM investigation was carried out in order to reveal the deep crystal structure of the silver dendrites. Figures 1c and d show typical silver dendrite structures at different magnifications. The results are consistent with those observed by using SEM. Figure 1e shows the detailed HRTEM structure of the Ag trunk, which clearly exhibits that the lattice fringes spacing is 0.23 nm. This matches the interplanar spacing of (111) of face centered cubic (fcc) silver. It indicates that the growth direction of the trunk is along (111).³⁶ Like Fig. 1e, the HRTEM image of the silver dendrites in Fig. 1f also shows that the connection site between trunk and one of its branches has lattice fringes spacing of about 0.23 nm. The branch growth

direction is also along (111). This implies that the Ag dendrites grow along a preferential direction, which agrees with the “oriented attachment” growth mechanism.³⁷ This is the main path for the formation of Ag dendrites. In addition, this HRTEM image also shows that the total dendrite structure is a single crystal, due to the fact that the trunk and the side branch have identical crystal orientations.³⁶

Figure 2 shows a typical x-ray diffraction (XRD) pattern of the silver dendrite products. The five diffraction peaks can be assigned to the (111), (200), (220), (311) and (222) planes of the fcc silver (according to the PDF2-2004 card). The strong and sharp diffraction peaks indicate that the silver

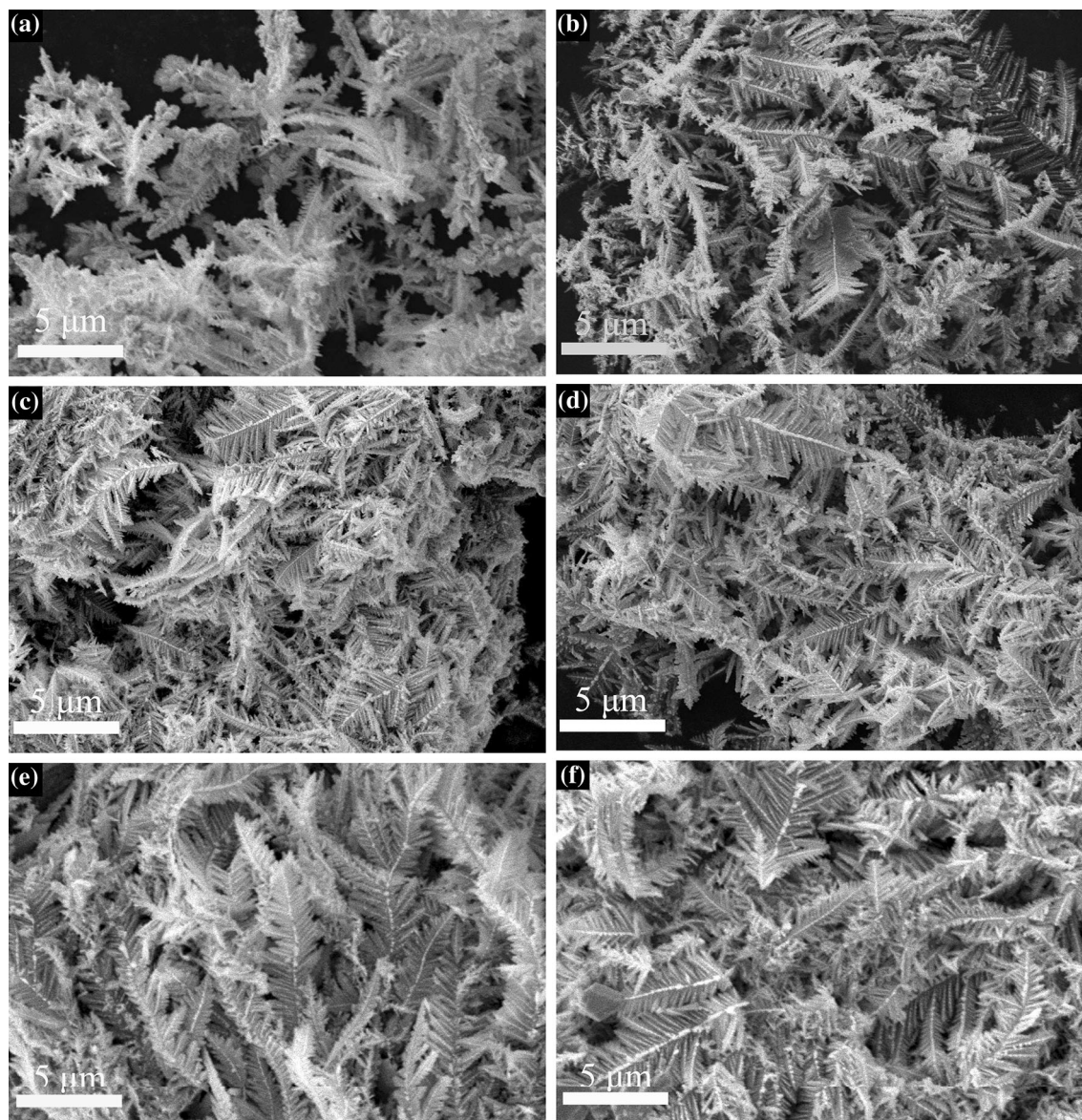


Fig. 6. SEM images of silver dendrites grown at the following reaction times: (a) 1 h, (b) 2 h, (c) 3 h, (d) 4 h, (e) 5 h, and (f) 6 h. Other experimental parameters are the same, reactant molar ratio is 4:1, reaction solution volume is 40 mL, and silver nitrate concentration is 30 mM.

dendrites are well crystallized. The intensity of the diffraction peak (111) is much stronger than the other peaks, which indicates that the silver dendrites are primarily dominated by the crystal facet (111), and the crystal growth direction is preferentially oriented parallel to the (111) direction. This result is consistent with the results of the HRTEM measurements.

Effect of Molar Ratio of Silver Nitrate and Zinc Powder on the Silver Dendrites Morphology

SEM images were taken in order to observe the shape transformation of the as-synthesized silver dendrites at different molar ratios of silver nitrate and zinc powder. As shown in Fig. 3, it is clear that

the mole ratio of silver nitrate and zinc powder heavily influences the morphology of silver dendrites.

The theoretical mole ratio of silver nitrate and zinc powder in the replacement reaction is 2:1. Based on this ratio, synthesized dendrites have the morphology shown in Fig. 3b, which clearly shows that besides the silver dendrites, some hexagonal silver is still left in the solution. The trunk and branch are usually loose and tiny, and the morphology ensemble of the silver dendrites is heterogeneous. When the molar ratio is reduced to 1:1 (Fig. 3a), the quantity of complete silver dendrites is reduced. In this reaction, zinc powder was used as a reducing agent. Excess zinc powder can accelerate the reaction rate, as AgNO_3 is rapidly reduced to Ag

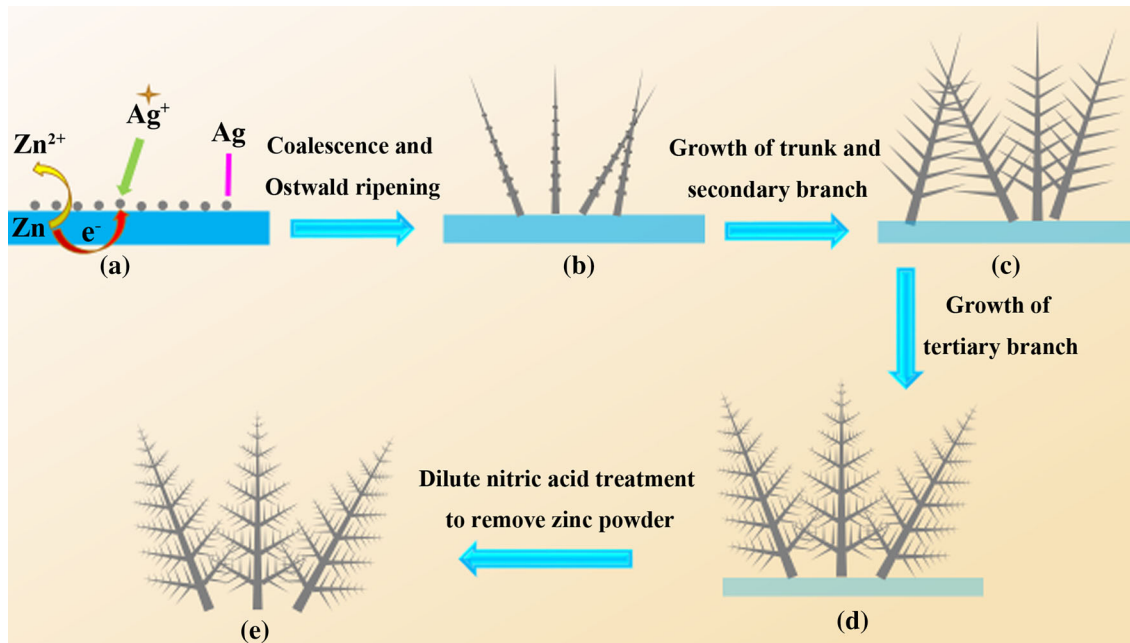


Fig. 7. Schematic illustration of the formation process of silver dendrites. (a) The replacement reaction between silver nitrate and zinc powder is carried out and Ag⁺ is reduced to Ag. (b–d) Growth process of trunk and branch of silver dendrites. (e) Removal of residual zinc powder to obtain purified silver dendrites.

atoms via replacement reaction. Subsequent free Ag atoms aggregate to form dendrites. As the reaction proceeds, the silver ion concentration drops to a certain level and the aggregation process slows down so that the silver has sufficient time to relax and seek the minimum energy position.³⁸ That is one tentative explanation for the observed transition from dendrites to a more compact hexagonal structure.³⁹ When the molar ratio is 4:1 (Fig. 3c), the amount of reducing agent is reduced. This decreases the reduction rate of the silver nitrate. The slowly precipitated Ag atoms promote the growth of silver dendrites, and the resulting silver dendrites are complete and symmetrical. The length of each trunk is about 5–10 μm , and the longest branch is around 1–2 μm in the middle of the trunk. The leaves have lengths of 100–300 nm. Therefore, it is essential to find the appropriate reactant ratio for the preparation of silver dendrites.

Effect of Reaction Solution Volume on the Morphology of Silver Dendrites

The effect of reaction solution volume on the morphology of silver dendrites can be seen in Fig. 4. It is clear that the dendrites are highly symmetric, and the angles between the trunk and the branch are approximately 50°–60° when the volume of the reaction solution is 40 mL (Fig. 4a). Moreover, the morphology of the silver dendrites is uniform. With an increase of the reaction solution volume (Fig. 4b–f), silver dendrites are generated but the shapes and symmetries are not as perfect

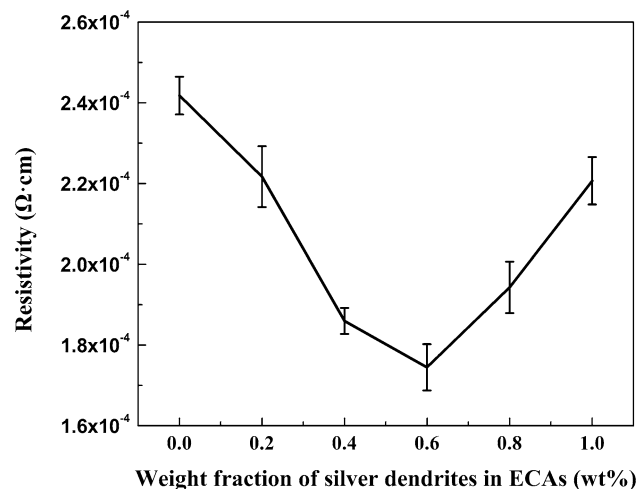


Fig. 8. Resistivity of ECAs changing trend under different weight fraction of silver dendrites.

before, as shown in Fig. 4e and f. There, it is difficult to find any dendrite with complete tree-like structure, while some silver particles start to show up in Fig. 4f. Apparently, when the volume of the reaction solution is increased, the zinc powder does not disperse uniformly in the solution, resulting in the disordered growth of silver dendrites. The larger the reaction solution volume, the more heterogeneous the morphology of the silver dendrites becomes.

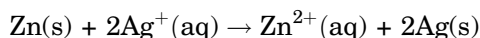
Effect of Silver Nitrate Concentration on the Morphology of Silver Dendrites

The silver dendrites' morphology is highly sensitive to the silver ion concentration. As shown in Fig. 5a and b, when the silver ion concentration is less than 30 mM, small and short silver dendrites begin to grow, with few branches and small diameters. When the concentration reaches about 30 mM, the silver dendrites start to show nearly perfect symmetric structure. A complete and well-defined dendritic structure arranged along a backbone with symmetrical side branches is observed in Fig. 5c. As the silver ion concentration is increased up to 50 mM, 100 mM, or 200 mM, the morphology of the silver dendrites becomes more and more asymmetric. It should be noticed that a small amount of hexagonal silver accumulation is detected. This implies that homogeneous morphology cannot be obtained when the silver ion concentration is too high, due to the quick reaction rate.⁴⁰ By controlling the silver ion concentration, silver dendrites with well-defined morphology and crystalline structure can be realized.

Effect of Reaction Time on the Morphology of Silver Dendrites

The growth of dendritic structure is literally a time-dependent process. Figure 6 shows the growth process of silver dendrites with different reaction times. When the reaction time is 1 h, a rod-like structure is formed (Fig. 6a). This indicates that the initial stages of the dendritic growth started from the main trunk. After 2–4 h (Fig. 6b and d) a rudimentary dendritic structure is formed. The silver dendrites have 3–5 μm long central Ag trunks with 0.5–1 μm secondary and small tertiary branches. When the reaction time reached 5–6 h (Fig. 6e and f), the dendrites extended vertically and laterally. Silver dendrites tend to grow larger and larger with the increase of reaction time. The trunk can grow up to 5–10 μm with secondary branches of 1–2 μm , and tertiary branches 100–300 nm in length.

Based on the above experimental measurements, we can speculate about a possible formation process. A schematic illustration of the silver dendrites formation process is presented in Fig. 7. Considering the fact that the standard electrode potential of the Ag^+/Ag (+0.799 V) is larger than that of Zn^{2+}/Zn (–0.762 V), the replacement reaction can be described as follows:



When the zinc powder is added into an AgNO_3 aqueous solution, Ag^+ is reduced to Ag^0 . After the Ag atoms are formed, they further aggregate to form Ag nanoparticles. Meanwhile, experiencing coalescence and Ostwald ripening,⁴¹ nanoparticles grow

and coalesce to rod-like structures, which appear as the formation of the initial silver dendrite structures. Other secondary branches will extend from the Ag trunk as time passes, and evenly grow into tertiary Ag branches. Eventually the larger and smoother silver dendrites structures are formed. During the reaction, Ostwald ripening plays a critical role in forming the smooth surface and a regular shape of the final crystal.⁴²

The Electrical Properties of Silver Dendrites Filled ECAs

ECAs that were filled with only silver flakes were used as control samples; they had a resistivity of $2.4 \times 10^{-4} \Omega \text{ cm}$. The electrical properties of the binary Ag/epoxy hybrid adhesives are presented in Fig. 8. It is interesting to find that the conductive properties of the ECAs are increased with the doping of the silver dendrites. The porosity of ECAs under different sample compositions is listed in Supplementary Figure S1.

The optimal filling amounts of silver flakes and silver dendrites are 69.4 wt.% (20.82 vol.%) and 0.6 wt.% (0.18 vol.%) respectively. The mass ratio of silver flakes to silver dendrites is 347:3. The corresponding resistivity reaches to $1.7 \times 10^{-4} \Omega \text{ cm}$. By theoretical calculation (see supporting information page 4), we know that the resistivity can reach $1.3 \times 10^{-4} \Omega \text{ cm}$ when 70.0 wt.% (21.00 vol.%) silver is filled in ECAs. The calculated values show good agreement with the measured values. Therefore, we can effectively estimate the resistivity of ECAs by calculation, which will be helpful for future experiments.

From Fig. 8, it can be seen that the resistivity of the ECAs first decreases and then goes up with the increase of the mass fraction of silver dendrites. In fact, the electrical conductivity of the ECAs highly depends on the formation of conductive networks established by silver flakes and silver dendrites. When a small amount of silver dendrites were added into the ECAs, silver dendrites were more likely to form conductive pathways by overlapping with each other due to their tree-like structure, and the silver dendrites could then connect the unattached silver flakes. With the increases of the concentration of silver dendrites, more conductive pathways are established, when it reaches the threshold a sharp decrease in the tunneling resistance appears.⁴³ However, when the content of silver dendrites gets too high, its non-uniform dispersion in the matrix resin creates an adverse effect on the conductive pathways.^{13,44} Silver dendrites cannot perfectly connect the gap between the silver flakes. Therefore, the number of conductive pathways is reduced, which leads to an increase in the tunneling resistance. At the same time, the number of contact points among conductive Ag fillers increases as the silver dendrite content increases. This leads to an increase of constriction

resistance.^{43,45} The competition of all those mechanisms is expressed as the silver dendrite-dependent electric properties of ECAs that we observed experimentally. The results above indicate that the proper mass fraction of silver flakes and dendrites can effectively improve the electrical conductivity of the conventional ECAs.

CONCLUSIONS

To summarize, a simple and efficient approach was developed to fabricate silver dendrites by replacement reaction. The perfect silver dendrite structures are obtained by carefully tuning the experimental parameters in the replacement reaction. The optimized preparation conditions are as follows: a molar ratio of silver nitrate to zinc powder of 4:1, reaction solution volume of 40 mL, silver nitrate concentration of 30 mM and a reaction time of 6 h. ECAs with low electrical resistivity were successfully created by doping with silver dendrites. The as-prepared binary Ag/epoxy ECAs show excellent conductive properties which are better than those of conventional ECAs filled with equal amounts of single silver flakes only. This result is attributed to the silver dendrites possessing relatively higher aspect ratios, which can establish many more conductive pathways in the polymer matrix than silver flakes. The optimal mass fractions of silver flakes and silver dendrites are 69.4 wt.% (20.82 vol.%) and 0.6 wt.% (0.18 vol.%), respectively, and the corresponding mass ratio of silver flakes to silver dendrites is 347:3. It was possible to obtain a resistivity of the ECAs as low as $1.7 \times 10^{-4} \Omega \text{ cm}$. We believe that the use of hybrid filler systems that use silver dendrites as auxiliary fillers is a promising approach to minimizing the resistivity of conventional Ag flake-filled ECAs.

ACKNOWLEDGEMENTS

This work was financially supported by Program for Changjiang Scholars and Innovative Research Team in University (PCSIRT, No. IRT1161), Program of Science and Technology Innovation Team in Bingtuan (No. 2011CC001). The work was also financially supported by the National Natural Science Foundation of China (No. 11774255), the Key Project of Natural Science Foundation of Tianjin City (No. 17JCZDJC30100) and the Innovation Foundation of Tianjin University (No. 2017XZC-0090).

ELECTRONIC SUPPLEMENTARY MATERIAL

The online version of this article (<https://doi.org/10.1007/s11664-018-6145-5>) contains supplementary material, which is available to authorized users.

REFERENCES

1. S. Joseph, G.J. Phatak, T. Seth, K. Gurunathan, D.P. Amalnerkar, T.R.N. Kuty, in *IEEE Conference on Convergent Technologies for the Asia-Pacific Region* (2003), pp. 1367–1371.
2. Y. Li, K.S. Moon, and C.P. Wong, *Science* 308, 1419 (2005).
3. Y. Li and C.P. Wong, *Mater. Sci. Eng. R Rep.* 51, 1 (2006).
4. I. Krupa, V. Cecen, A. Boudenne, J. Prokes, and I. Novak, *Mater. Des.* 51, 620 (2013).
5. L.N. Ho and H. Nishikawa, *J. Mater. Sci. Mater. Electron.* 26, 7771 (2015).
6. H.R. Ma, M.Z. Ma, J.F. Zeng, X.H. Guo, and Y.Q. Ma, *Mater. Lett.* 178, 181 (2016).
7. J. Li, J.K. Lump, in *2006 IEEE Aerospace Conference* (2006), pp. 2521–2526.
8. Y.H. Wang, N.N. Xiong, Z.L. Li, H. Xie, J.Z. Liu, J. Dong, and J.Z. Li, *J. Mater. Sci. Mater. Electron.* 26, 7927 (2015).
9. H. Van Luan, H.N. Tien, T.V. Cuong, B.S. Kong, S.C. Jin, E.J. Kim, and S.H. Hur, *J. Mater. Chem.* 22, 8649 (2012).
10. B.M. Amoli, A. Hu, N.Y. Zhou, and B. Zhao, *J. Mater. Sci. Mater. Electron.* 26, 4730 (2015).
11. I. Mir and D. Kumar, *Int. J. Adhes. Adhes.* 28, 362 (2008).
12. X. Peng, F.T. Tan, W. Wang, X.L. Qiu, F.Z. Sun, X.L. Qiao, and J.G. Chen, *J. Mater. Sci. Mater. Electron.* 25, 1149 (2014).
13. Y.H. Ji, Y. Liu, G.W. Huang, X.J. Shen, H.M. Xiao, S.Y. Fu, and A.C.S. Appl, *Mater. Interfaces* 7, 8041 (2015).
14. D.P. Chen, X.L. Qiao, X.L. Qiu, F.T. Tan, J.G. Chen, and R.Z. Jiang, *J. Mater. Sci. Mater. Electron.* 21, 486 (2010).
15. L.H. Fan, B. Su, J.M. Qu, and C.P. Wong, *Electron. Compon. Technol. Conf.* 1, 148 (2004).
16. P. Mach, R. Radev, and A. Pietrikova, in *Electronics System-Integration Technology Conference* (2008), p. 1141.
17. Z.X. Zhang, X.Y. Chen, and F. Xiao, *J. Adhes. Sci. Technol.* 25, 1465 (2011).
18. C. Chen, L. Wang, R.L. Li, G.H. Jiang, H.J. Yu, and T. Chen, *J. Mater. Sci.* 42, 3172 (2007).
19. S. Gupta and R. Prakash, *Rsc Adv.* 4, 7521 (2014).
20. M.H. Rashid and T.K. Mandal, *J. Phys. Chem. C* 112, 1304 (2008).
21. L.D. Rafailovic, C. Gammer, J. Srajer, T. Trisovic, J. Rahel, and H.P. Karnthaler, *Rsc Adv.* 6, 33348 (2016).
22. C. Yang, X.Y. Cui, Z.X. Zhang, S. Chiang, W. Lin, H. Duan, J. Li, F.Y. Kang, and C.P. Wong, *Nat. Commun.* 6, 8150 (2015).
23. X. Qin, Z.Y. Miao, Y.X. Fang, D. Zhang, J. Ma, L. Zhang, Q. Chen, and X.G. Shao, *Langmuir* 28, 5218 (2012).
24. C.D. Gu and T.Y. Zhang, *Langmuir* 24, 12010 (2008).
25. M.V. Mandke, S.H. Han, and H.M. Pathan, *CrystrEngComm* 14, 86 (2012).
26. B. Keita, L.R.B. Holze, R.N. Biboum, L. Nadjjo, I.M. Mboemekalle, S. Franger, P. Berthet, F. Brisset, F. Miserque, and G.A. Ekeidi, *Eur. J. Inorg. Chem.* 2011, 1201 (2011).
27. L. Wang, H.L. Li, J.Q. Tian, and X.P. Sun, *ACS Appl. Mater. Interfaces.* 2, 2987 (2010).
28. G.D. Wei, C.W. Nan, Y. Deng, and Y.H. Lin, *Chem. Mater.* 15, 4436 (2003).
29. J.P. Xiao, Y. Xie, R. Tang, M. Chen, and X.B. Tian, *Adv. Mater.* 13, 1887 (2001).
30. P. Gao, M. Zhang, H. Hou, and Q. Mao, *Mater. Res. Bull.* 43, 531 (2008).
31. Z.J. Wang, F. Tao, D.B. Chen, L.Z. Yao, W.L. Cai, and X.G. Li, *Chem. Lett.* 36, 672 (2007).
32. J.X. Fang, H.J. You, P. Kong, Y. Yi, X.P. Song, and B.J. Ding, *Cryst. Growth Des.* 7, 864 (2007).
33. Z.Y. Jiang, Y. Lin, and Z.X. Xie, *Mater. Chem. Phys.* 134, 762 (2012).
34. L. Polavarapu, K.K. Manga, H.D. Cao, K.P. Loh, and Q.H. Xu, *Chem. Mater.* 23, 3273 (2011).
35. T. Akter and W.S. Kim, *ACS Appl. Mater. Interfaces.* 4, 1855 (2012).
36. G.X. Zhang, S.H. Sun, M.N. Banis, R.Y. Li, M. Cai, and X.L. Sun, *Cryst. Growth Des.* 11, 2493 (2011).
37. R.L. Penn and J.F. Banfield, *Science* 281, 969 (1998).

38. J.X. Fang, X.N. Ma, H.H. Cai, X.P. Song, B.J. Ding, and Y. Guo, *Appl. Phys. Lett.* 89, 173104 (2006).
39. J.X. Fang, H.J. You, C. Zhu, P. Kong, M. Shi, X.P. Song, and B.J. Ding, *Chem. Phys. Lett.* 439, 204 (2007).
40. X.J. Zhang, R. Ji, L.L. Wang, L.T. Yu, J. Wang, B.Y. Geng, and G.F. Wang, *CrystEngComm* 15, 1173 (2013).
41. M. Jose-Yacamán, C. Gutierrez-Wing, M. Miki, D.Q. Yang, K.N. Piyakis, and E. Sacher, *J. Phys. Chem. B* 109, 9703 (2005).
42. C. Fang, Y. Fan, J.M. Kong, Z.Q. Gao, and N. Balasubramanian, *Appl. Phys. Lett.* 92, 263108 (2008).
43. B.M. Amoli, E. Marzbanrad, A. Hu, Y.N. Zhou, and B.X. Zhao, *Macromol. Mater. Eng.* 299, 739 (2014).
44. H.R. Ma, J.F. Zeng, S. Harrington, L. Ma, M.Z. Ma, X.H. Guo, and Y.Q. Ma, *Nanomaterials* 6, 119 (2016).
45. R. Taherian, M.J. Hadianfard, and A.N. Golikand, *J. Appl. Polym. Sci.* 128, 1497 (2013).